AMERICAN
METEOROLOGICAL
SOCIETY

Bulletin of the American Meteorological Society

The DOI for this manuscript is doi: 10.1175/BAMS-D-11-00194.1

Orographic Precipitation in the Tropics:

The Dominica Experiment

Ronald B. Smith, Justin Minder, Alison Nugent, Trude Storelvmo

(Department of Geology and Geophysics, Yale University)

Daniel J. Kirshbaum

(Department of Atmospheric and Oceanic Sciences, McGill University)

Robert Warren

(Dept. of Meteorology, University of Reading),

Neil Lareau

(Dept. of Atmospheric Sciences, University of Utah)

Philippe Palany

(MeteoFrance, Martinique)

Arlington James

(Forestry Division, Dominica)

Jeffrey French

(Dept. of Atmospheric Science, U. Wyoming)

Submitted November 1, 2011 (Revision Feb 29, 2012)

Corresponding Author:

Professor Ronald B. Smith
Dept. of Geology and Geophysics
Yale University
P.O. Box 208109
New Haven, CT
06520-8109

Office: (203)432-3129
ronald.smith@yale.edu

Abstract: The Dominica Experiment (DOMEX) took place in the eastern Caribbean from April 4 to May 10, 2011 with 21 research flights of the Wyoming King Air and several other observing systems. The goal was an improved understanding of the physics of convective orographic precipitation in the tropics. Two types of convection were found. During a period of weak trade winds, diurnal thermal convection was seen over Dominica. This convection caused little precipitation but carried aloft air with island-derived aerosol and depleted CO_2. During periods of strong trades, mechanically forced convection over the windward slopes brought heavy rain to the high terrain. This convection was "seeded" by trade wind cumuli or neutrally buoyant cool wet patches of air. In this mechanically-forced convection, air parcels did not touch the island surface to gain buoyancy so no island derived tracers were lofted. With fewer aerosols, the mean cloud droplet diameter increased from 15 to 25microns. Plunging airflow and a wake were found in the lee of Dominica. The DOMEX data set will advance our understanding and test our theories of cumulus triggering and aerosol influence on precipitation.

Capsule:

The surprising sensitivity of the wind field, aerosol concentration, cloud physics and precipitation over Dominica to trade wind speed arises from a switch-over between thermally and mechanically triggered convection and between non-plunging and plunging airflow.

1. Introduction

Orographic precipitation influences water resources, flooding and landslides, regional climates and global water budgets. Furthermore, the study of mountain-induced lifting and precipitation serves as a prototype for the study of other types of airmass lifting in the atmosphere (e.g. frontal, cold pool, dryline). Until now, orographic precipitation has been widely studied only in mid-latitudes with field projects such as Sierra Cooperative Pilot project (SCPP), The Alpine Experiment (ALPEX) , Southern ALPEX (Wratt, 1996), Improve (Stoelinga et al. 2003), Mesoscale Alpine Programme (MAP: Bougeault et al. 2001, Rotunno and Houze , 2007), Cupido (Geerts et al. 2009) and others. Summaries can be found in Smith (1979, 2007), Roe (2005), Houze (2011). Mountain effects in the subtropics have been studied in Taiwan and Hawaii (e.g. Kuo and Chen, 1990; Yang and Chen, 2008). These locations still have some mid-latitude climatic influences and under typical conditions airflow goes around rather than over these tall terrains. Progress has also been made on thermally driven island convection in the tropics (e.g. Carey and Rutledge, 2000; Wilson et al. 2001; Sobel et al. 2010; Robinson et al, 2011). In contrast, the Dominica Experiment was designed to study orographic precipitation in the tropics with cumulus triggering by forced ascent in unblocked flow.

Dominica (15N, 61W) lies in the eastern Caribbean in the Lesser Antilles chain of volcanic islands (Fig 1). Its terrain is dominated by the 1.4 km peaks of Mt Diablotin in the north and Trois Piton in the south. Between the peaks is a saddle with an elevation of 600m. Orographic precipitation is a key issue for Dominica. It generates about half of its electricity from hydropower and there are plans to export bulk fresh water to dryer Caribbean islands. Frequent heavy rain events cause flooding and landslides on the island. From many interesting sites in the tropics, Dominica was selected as our natural laboratory for the following reasons: heavy convective orographic precipitation (Fig 2), steady tradewind flow, unobstructed upstream environment, simple twin-peak terrain, two off-island French

radars, nearby balloon soundings and road access to high mountain sites. Previous studies of the tropical Atlantic in BOMEX (Holland and Rasmussen, 1973), RICO (Rauber, et al. 2007) and BACEX (B. Albrecht, personal communication, 2010) helped to define the upstream physical environment for Dominica.

The Dominica Experiment (DOMEX) took place in two phases. From 2007 to 2011, data from installed rain gauges, the Guadeloupe radar and soundings (TFFR) were studied to understand the climatology of the island (Smith et al, 2009a). The orographic enhancement associated with the passage of Hurricane Dean was also studied with these instruments (Smith et al 2009b). Modeling and theoretical studies were carried out as well (Kirshbaum and Smith, 2009; henceforth KS09).

From these studies, several general attributes of the precipitation climate of Dominica were established. The orographic enhancement factor, defined as the ratio of precipitation on the high terrain to upstream, varies from 2 to 12 depending on conditions. The smaller factor applies to days with substantial rain over the ocean upwind. While enhancement begins a few kilometers upwind of the east coast, it is focused primarily on the highest terrain. The high peaks receive nearly 6 meters of rain each year compared to 0.5 meters upwind (Fig. 2). The rain typically comes in ten minute showers from liquid-only “warm” clouds extending to an altitude of 3 to 4km. A very sharp rainfall gradient is present on the lee slopes. The west coast and the adjacent ocean in the lee of the terrain experience less than 20 centimeters of annual rainfall. This strong “rain shadow” is not caused by water vapor depletion as the annually averaged Drying Ratio (i.e. the ratio of total rainfall to incoming water vapor flux) is less than 0.5%. Instead, the rain shadow is probably caused by lee side descent, dry air entrainment or increased static stability. While many larger tropical islands experience a diurnal cycle in precipitation driven by solar heating, this type of modulation is very small on Dominica. On normal to strong tradewind days, it seems that mechanically forced ascent rather than solar heating triggers the

convection and precipitation. To address these and other issues, a second phase of DOMEX was designed; DOMEX2011.

2. The DOMEX-2011 field campaign

The goals of DOMEX-2011 were: 1) To understand the physics of mountain triggered convection and precipitation in the tropics, using Dominica as a natural laboratory, 2)To develop data sets that can be used to test and improve numerical models of convection and precipitation in the tropics, and 3) To better understand and predict the weather and climate of the Lesser Antilles including Guadeloupe, Dominica and Martinique. The DOMEX-2011 field phase (April 4 to May 10, 2011) in the dryer season allowed a focus on orographic precipitation without the complications associated with organized tropical distrubances. The key observing system was the Wyoming King Air research aircraft with the capability to measure flight level winds, thermodynamics, carbon dioxide, aerosol and cloud particles. These quantities were recorded at a rate of 25 Hz which, with an airspeed of $90m\ s^{-1}$, gave a sampling distance of about 4 meters. In addition, the King Air carried the 95GHz Wyoming Cloud Radar (WCR) and the 355nm Wyoming Cloud Lidar (WCL; Wang et al. 2009). The National Science Foundation allocated 80 flight hours to DOMEX-2011 allowing 21 flights (Table 1). The King Air flew out of the Aime Cesaire airport in Lamentin on nearby Martinique.

The King Air flight pattern consisted of an upstream sounding and six horizontal legs (Fig 3). An upwind sounding was taken at the start of each flight from an altitude of 4000m down to 150m. Legs 1,2 and 5 were flown over the ocean at two altitudes: 300m and 1200m. Leg 1 observed undisturbed upstream conditions while Leg 2 observed any changes in the airflow reaching the Dominican coast. Leg 2 had a “dogleg” shape to keep it close to the coast.

The surface instrumentation on Dominica was enhanced for DOMEX-2011. The number of rain gauges across the southern peaks was increased to ten. A satellite-linked weather station was installed on an east-facing ridge near Freshwater Lake (Fig 3). A small section of hill-top forest was cleared to provide acceptable wind observations with a 6 meter tower. Standard meteorological variables were recorded with two minute resolution. Three web cameras were installed on the east and west coasts for continuous time lapse photography with 30 second resolution. The camera at Rosalie on the east coast faced eastward. The two cameras in Roseau on the west coast faced eastward and northward. A Joss-Waldvogel disdrometer was installed at Rosalie. With the assistance of NCAR, GOES sector images were captured and archived. The MeteoFrance Guadeloupe balloon sounding frequency was increased from once to twice per day. Data from four MeteoFrance surface stations were archived with 6-minute time resolution. Scans from Guadeloupe and Martinique 2.8GHz weather radars were recorded every five minutes. Hourly surface meteorological data are available from the two airports on Dominica: Melville Hall and Canefield.

3. Role of trade wind speed

The twenty one cases flown with the King Air varied considerably in their ambient trade wind speed, wind direction, humidity, upstream precipitation and other parameters (Fig 4). Any attempt to fully categorize these cases would probably require a multi-dimensional parameter space. To a first approximation however, it appears that the wind speed is the dominant upstream control parameter. To illustrate the role of wind speed, we plot four over-island parameters versus upstream wind speed in Figure 5. The standard deviation of vertical wind speed over the eastern slope (Fig 5a, Leg 3) shows a non-monotonic behavior. We interpret this pattern as evidence of two modes of convection. For wind less than $5m\ s^{-1}$, the convection is thermally driven. For winds between $5m\ s^{-1}$ and $8m\ s^{-1}$, the convection is weak. We propose that the wind suppresses the thermal convection while the wind is still

too weak to mechanically force energetic convection. When the wind exceeds $8m\ s^{-1}$,the mechanically forced convection is strong. The straight line in Fig 5a shows a possible relationship between wind speed and convective amplitude by mechanical forcing as proposed by KS09.

The aerosol and cloud number concentrations trend downward with wind speed in Figs 5b and 5c. As shown below, this trend is probably due to island-derived aerosol carried upward in the thermal convection. Mechanically driven convection in the strong wind cases does not elevate this aerosol. In figure 5d, the difference in wind between Legs 3 and 4 at z=1700m is plotted versus wind speed. In low wind cases, the difference is positive indicating diverging flow from the cloud top detrainment. In high wind cases, the difference is negative indicating that the easterly flow found on Leg 3 plunges beneath Leg 4 (see section 8).

To further illustrate the role of wind speed, we have identified four high wind cases ($U > 8m\ s^{-1}$) and two low wind cases ($U < 5m\ s^{-1}$) that have common characteristics. Their general flow properties are summarized in Table 1.

[Table 1]

The upstream wind direction, dry and moist stabilities and reverse shear are similar for the low and high wind cases. The dry Brunt-Vaisala frequency above cloud base is about $N = 0.012s^{-1}$. The equivalent potential temperature decreases by about 20 degrees from z=500 to 3500m indicating conditional instability. The upstream conditions differ most in the low level wind speed and the height of the wind reversal.

The non-dimensional mountain height $\hat{h} = Nh/U$ is 0.9 in the high wind case and 3.2 in the low wind case. In the latter case one would expect the airflow to deflect around the mountain (Smith, 1979), but this is not observed. Perhaps the thermal heating of the slopes or the latent heat aloft draws air up

the eastern slopes and keeps the air moving towards the east coast of the island (Reisner and Smolarkiewicz, 1994). The adiabatic layer beneath cloud base may also help the air to lift and avoid deceleration.

The convection over the island seems to be of two types, as shown in Table 1. The cloud fraction is greater at flight level over the eastern slopes (Leg 3) for high wind case but greater over the western slopes (Leg 4) for the low wind case. This shift in convection location is not clear in the standard deviation of w', as clear air turbulence associated with plunging flow on Leg 4 can be as strong as the convection. The shift in convection location is more clearly seen in vertical velocity skewness $S = \int (w')^3 \, dx / \left[\int (w')^2 dx\right]^{3/2}$ and the latent heat flux (Table 1). Positive skewness indicates that the updrafts are narrow and strong with weak broad downdrafts; a characteristic of moist convection. The legs with larger skewness also have larger latent heat flux, confirming the shift in convection with wind speed (Table 1).

It is perhaps counter intuitive that the weaker wind case would push the convection further west than the high wind case, but this discovery reinforces the idea that two different convection mechanisms are at work. The strong wind case generates convection over the windward slope (Leg 3) with the mechanical ascent mechanism and suppresses lee convection with descent. In the weak wind case, warm thermal boundary layer flow is pushed westward to the vicinity of Leg 4 by the prevailing winds. Judging from the latent heat fluxes, the weak wind convection is at least as strong as the strong wind convection.

Another distinct difference between the high and low wind cases is seen in the cloud particle properties (Table 1). In the weak wind cases, due to lofted island aerosol (See Section 7), the cloud number concentration is large and the mean droplet size is small. The smaller droplet size could explain the lighter precipitation seen in the weak wind cases. It may be more difficult for collision-coalescence

to grow raindrops (e.g. Warner, 1968; Gunn and Phillips, 1957; Blanchard and Spencer, 1957). This difference in droplet size is similar to those found in recent numerical simulations of clouds in clean and polluted air (Morrison and Grabowski, 2007; Muhlbauer and Lohmann, 2008). In this environment however, the effects of hygroscopic nuclei (e.g. Jensen and Lee, 2008) and turbulence (e.g. Wang and Grabowski, 2009) must also be considered. Differences in cloud depth and dry air entrainment should also be considered.

The role of wind speed can be further illustrated by comparing two flights with contrasting wind speed. Research flight 7 on April 18 had weak tradewinds of about $2m\ s^{-1}$ with westerlies above 1500m (Fig 6a). Research flight 13 on April 27 had stronger tradewinds of nearly $12m\ s^{-1}$ with westerlies above 3500m (Fig 6b). Photographs of the two cloud systems are shown in Fig 7 and the precipitation patterns are in Fig 8. Aloft at 1700 m, the two cases had different wind fields. In the weak wind case, Legs 3 and 4 show a divergence associated with detrainment from the cumulus line (Fig 9a). In the fast wind case, Legs 3 and 4 show a convergence (Fig 9b). The fast air found along Leg 3 drops below Leg 4 and stagnant and slow turbulent air is found on Leg 4 (Smith, 1987).

The Wyoming Cloud Radar shows the vertical distribution of large cloud droplets and small raindrops. Over the eastern windward slope (Leg 3), the radar shows more cells and stronger reflectivity on the strong wind day (Fig 10). Over the western slopes (Leg 4), the radar shows weak updrafts on the weak wind day but suppressed convection and a 600 meter deep layer of spillover rain on the strong wind day (Fig 11).

The mean droplet size in high wind case (RF13) is compared with the slow wind case (RF07) in Fig 12. This diagram includes all the cloud penetrations over the island for each flight. The probability peak occurs at diameters of 15 and 25 microns for the slow and fast wind cases respectively. We argue below that the droplet size is influenced by island derived aerosols.

4. Island derived tracers

The aerosol distribution along Legs 3 and 4 are shown in Fig 13 for the weak and high wind examples (i.e.RF07 and RF13). In this figure, the aerosol number concentration and CO_2 concentration are plotted versus time while the aircraft flies two complete "racetrack" circuits around Legs 3, 4, 3, 4 at z=1700m (see Fig 3). Brief cloud penetrations are excluded from these plots so the data represents air outside of clouds. At the northern and southern ends of the racetrack, the aircraft is outside of the influence of the island, so the observations represent the undisturbed environment. In the middle of Legs 3 and 4, the aircraft flies though the detraining air from clouds over the island. For RF07, the aerosol number concentration over the island rises well above the ambient level while for RF13, the aerosol concentration is constant along each leg.

Our interpretation is as follows. In the case of thermal convection in weak ambient wind (e.g. RF07), the air detraining from the plume must have come in contact with the island surface, or at least a shallow island boundary layer, in order to gain sensible heat and buoyancy. Using a diffusivity $K \approx 100 m^2 s^{-1}$, we estimate that the depth (d) of this internal boundary layer grows downwind of the coast and reaches $d = \sqrt{\frac{Kx}{U}} < 150\ meters$. Aerosols released from the island surface thereby provide a tracer of thermally driven convection. Conversely, in the case of mechanically driven convection during high winds (e.g. RF13), the plume buoyancy arises "internally" from latent heat release in moist parcels several hundred meters above the island surface. Air in these rising plumes shows no indication of contact with the island surface.

The carbon dioxide concentration provides an independent indication of air with recent contact with the island surface (Figs 13). In the detraining air over the island on Legs 3 and 4 on RF07, the CO_2

concentration drops below ambient by about two ppmv. We interpret this drop as evidence of air that has recently lost CO_2 by forest uptake on Dominica. A nearly identical pattern of island tracers is seen on the other weak wind case RF08. The other strong wind cases (i.e. RF12, 16, 17) show no island-derived tracers at 1700 m.

5. Upstream seeds of mechanically forced convection

Our theory of mechanically driven convection relies on the idea that the ambient upstream air contains clouds and other fluctuations in humidity (Woodcock, 1960; KS09). When the airstream is quickly lifted by the terrain, cloudy and dry air parcels ascend along different adiabats. After a few hundred meters of lift, significant differential buoyancy is generated and strong ascending plumes are created. With the aircraft data on Legs 1L and 1H in DOMEX2011, we have the possibility of observing the humidity seeds upstream of the island and possibly deducing their origin.

The upstream horizontal aircraft legs in DOMEX2011 are similar to many over-ocean research flights in previous projects (e.g. Bean et al., 1972; Donelan and Miyake, 1973). Our preliminary analyses of these legs confirm three interesting features seen in these earlier studies. First, while the latent heat fluxes are all positive, most of our sensible heat fluxes at 300m are negative (e.g. Nicholls and Lemone, 1980; Siebesma et al. ,2003). If the convection is locally driven, this result implies that the buoyancy force driving the sub-cloud convection comes from the difference in molecular weight between water vapor and air (i.e. the "virtual effect"). This is "compositional" convection rather than the usual "thermal" convection. Second, the horizontal scales of vertical velocity fluctuations differ greatly from the dominant scales of temperature and water vapor fluctuations (Nicholls and Lemone ,1980). Using lag autocorrelation, we found w-scales of 500 to 1000 meters but T-scales and q-scales of 3 to 8 km; almost a factor of ten difference. Third, in the upper part of the sub-cloud layer, the temperature and specific

humidity fluctuations are strongly anti-correlated (e.g. Shinoda et al., 2009). One explanation for this observation involves turbulent entrainment of potentially warm dry air at the top of the mixed layer, but Siebesma et al. (2003) did not see this in their marine boundary layer simulations. Alternatively, evaporation of falling rain might create cool moist patches (Paluch and Lenschow, 1991).

In this third respect however, our results differ from previous results. We note that not only are T and q anti-correlated, but their contributions to virtual temperature and air density nearly cancel. This is shown in Fig 14, where the scatter of points lies along a reference line for constant virtual temperature ($T_V = T + 0.61q$). Also, there is little vertical velocity on these scales. We wonder whether these neutral buoyancy patches are the remnants of old detrainment or cold pool events that underwent "buoyancy sorting". Dense parcels fell and less dense parcels rose until lateral buoyancy variations vanished. Once this adjustment has occurred, the patches drift along as passive tracers. Upon orographic lifting, they become dynamically active as the wet patches develop positive buoyancy. Their initial scale over the sea (i.e. 3 to 8km) may determine the scale of convection over Dominica.

6. **The Plunge and the Wake**

Over the lee slope of the island, clear evidence of descent and acceleration was found, even though the aircraft could not fly safely at low altitude. Clues to the descent were: 1) sloping cloud tops, 2) slow reverse flow along leg 4 indicating that the main airstream has gone plunged below, 3) clear air turbulence on Leg 4 from the strong reverse wind shear below, 4) cloud clearing near the coast, 5) dual Doppler measurements of accelerated flow below Leg 6 over the lee slope, 6) a rise in theta on Legs 4 and 6 associated with descent, 7) spillover of rain from upwind, 8) convergence of the horizontal wind vectors between Leg 3 and 4. By these criteria, plunging air was found on at least four of the DOMEX flights (RF 12,

13, 16 and 17). The Roseau cameras show a foehn-wall cloud over the ridgeline on those days, and a shallow high-speed layer of air moving downslope. On occasion, the plunging easterly flow persists all the way to Canefield airport on the west coast of Dominica (e.g. the period 1400 to 2200 UTC on April 27, 2011 including flight RF13).

The wake Legs 5L and 5H revealed wake structures on most strong flow flights. There were usually two or three wakes, each from a different mountain peak on Dominica. In addition, the air outside the wake was accelerated by several meters per second relative to the upstream wind speed. Preliminary analysis seems to confirm the hypothesis of Smith et al. (1997) that wakes have constant pressure but a Bernoulli function deficit. After correcting the pressure for diurnal and semidiurnal tidal oscillations and GPS-derived aircraft altitude changes, the pressure appears generally depressed to the west of Dominica but constant across the wakes themselves. This observation provides a partial explanation of both the general regional acceleration and the wake itself. The wake also has a deficit in carbon dioxide of 2ppmv, indicating that wake air has touched the forests of Dominica.

7. Conclusions

The strategy of using similar flight patterns around Dominica in different ambient flows helped us identify the role of trade wind speed. Two types of convection occur over Dominica, depending on the trade wind speed. Under weak trades ($U < 5m\ s^{-1}$), diurnal thermal convection occurs with the strongest updrafts located over the ridgeline and lee slopes (Fig 15a). Under strong trades ($U > 7m\ s^{-1}$), mechanically driven convection occurs with the strongest updrafts over the windward slopes

(Fig 15b). Under intermediate flow speeds ($5 < U < 7m\ s^{-1}$) the thermal convection is suppressed by the trade winds but the mechanically forced convection is still weak.

In the strong wind cases, the mechanically forced convection builds over the windward slope and brings heavy rain to the highest terrain. These clouds are quickly dissipated over the lee slope by plunging airflow. The lee slope environment is characterized by fast descending flow, clear air turbulence and raindrops spilling over from the windward side convection. Near the ridge ends, convection is still generated by the terrain but the plunging flow is absent, causing "book-end" convection. The mechanically forced convection is triggered either by upstream cumulus clouds or upstream sub-cloud moisture anomalies (KS09). The sub-cloud moisture anomalies are neutral patches with compensating temperature and humidity so that the virtual temperature is constant. We speculate that these patches result from buoyancy sorting in the upwind oceanic tradewind boundary layer.

Surprisingly, the nature of the convective triggering is reflected in the transport of island-source tracers. On strong wind days, plume buoyancy is probably generated a few hundred meters above the earth surface by the orographic lifting of ambient moisture anomalies. As these buoyant parcels never enter the island internal boundary layer, they do not gather island source tracers. In contrast, on weak wind days, plume parcels gain their buoyancy from the sun-heated island. Air detraining from these plumes, carries high aerosol and reduced carbon dioxide concentrations derived from the island surface.

Even more surprising is the impact of the aerosol tracer on cloud microphysics and precipitation. On weak wind days, with high island-derived aerosol concentration, the cloud droplet number density is much larger and the mean cloud droplet diameter much smaller than on the high-wind low-aerosol days i.e. 15 versus 25 microns). As a result perhaps, little precipitation falls from the convective clouds on the low wind days. This result is consistent with the lack of a climatological diurnal cycle in precipitation. While low wind days allow a diurnal cycle of convection to occur over Dominica, they contribute

minimally to the annual rainfall amount. Other factors that might suppress precipitation on weak wind days are dryer conditions aloft, reduced sea salt nuclei or the limited frequency of weak wind days.

Many questions remain unanswered about Dominica's airflow, clouds and precipitation. What is the role of upstream precipitation? Does the convection seeding come from the cloud or sub-cloud layer? What determines the scale of the convection? Does the plunging require a critical level in the upwind flow? How does the plunge dissipate the convection? What is the source of the island derived aerosol? How does the aerosol suppress precipitation? How is the wake generated? Our answers to these questions may improve short term forecasting in the eastern Caribbean.

A long term objective is to compare DOMEX results with orographic precipitation elsewhere in the tropics. Potential analogues to Dominica include the Central American Cordillera, the Western Ghats of India, the coastal range of Myanmar, the Philippines, Sumatra and Madagascar. There may also be analogues in mid-latitudes where conditionally unstable airstreams are lifted by terrain or by other means.

8. Acknowledgements

The DOMEX project was funded through the AGS Division at the USA National Science Foundation with advice from Brad Smull. The King Air participation was funded through the NSF deployment pool. The Yale staff were supported by a grant to Yale University (#0930356). The installation of instruments in Dominica was assisted by the Forestry Division (David Williams, Ashton Lugay), Met Office(Marshall Alexander), Agriculture (Rickey Brumant), Fisheries (Andrew Magloire, Derrick Theophile) and the Environmental Coordinating Unit (Collin Guiste), Grand Fond School (Mrs. Verna Frederick), Springfield Plantation (Nancy Osler). A camera and disdrometer were installed at Rosalie Bay Resort (Jan Neel, Ravey Sanchez). The disdrometer was loaned to us by Sandra Yuter. The Ports Authority (Benoit Bardouille) gave permission for flight operations over the island. On Martinique, MeteoFrance supported DOMEX in several ways including surface and radar data, daily weather briefings, extra 00Z soundings and office space. Thanks to Patrick Van Grunderbeeck, Daniele Carnino, Christian Massip, Niels Oger, Eloi Regina and others. The Wyoming King Air staff (Larry Oolman, Brett Wadsworth, Ahmad Bandani, Sam Haimov and others) provided a high level of support to the project. The aircraft and the airborne instruments worked reliably and the staff helped to solve several problems regarding instrument selection, flight track design, ATC clearances and variable weather conditions. Larry Bonneau at the Yale Center for Earth Observation helped with satellite images, maps and webcam installation. Greg Stossmeister and Glenn Randers-Pehrson assisted with GOES image archiving and animation. Bill Boos made useful suggestions for the research. Sigrid R-P Smith assisted with logistics.

9. References

Bean, B. R., C. Travis, R. McGavin, R. L. Grossman, and R. Gilmer, 1972: Analysis of Airborne Measurements of Vertical Water Vapor Flux During BOMEX. *J. Atmos. Sci*., **29**, 5, 860-869.

P. Bougeault, P. Binder, A. Buzzi, R. Dirks, J. Kuettner, R. Houze, R. B. Smith, R. Steinacker, H. Volkert, 2001, The MAP Special Observing Period, *Bulletin of the American Meteorological Society*, Volume 82, pp. 433-462
doi: 10.1175/1520-0477(2001)082<0433:TMSOP>2.3.CO;2

Blanchard, D. C. and A. T. Spencer, 1957: Condensation nuclei in the vicinity of the island of Hawaii. *Tellus*, **9**, 4, 525-527.

Carey, L. D. and S. A. Rutledge, 2000: The relationship between precipitation and lightning in tropical island convection: A C-band polarimetric radar study. *Mon. Wea. Rev.*, **128**, 8, 2687-2710.

Donelan, M., and M. Miyake, 1973: Spectra and fluxes in the boundary layer of the trade-wind zone. *J. Atmos. Sci*., **30**, 3, 444-464.

Geerts, B., Q. Miao, J. C. Demko, 2008: Pressure perturbations and upslope flow over a heated, isolated mountain. *Mon. Wea. Rev.*, **136**, 11 4272-4288.

Gunn, R., B. B. Phillips, 1957: An experimental investigation of the effect of air pollution on the initiation of rain. *J. Atmos. Sci*., **14**, 272-280.

Holland, J. Z., E. M. Rasmusson, 1973: Measurements of the atmospheric mass, energy, and momentum budgets over a 500-kilometer square of tropical ocean. *Mon. Wea. Rev.*, **101**, 1, 44-55.

Houze, R.A., 2011, Orographic effects on precipitating clouds, *Rev. Geophys*, In Press.

Jensen, J.B., and S. Lee, 2008: Giant sea-salt aerosols and warm rain formation in marine stratocumulus. *J. Atmos. Sci.*, **65**, 3678-3694.

Kirshbaum, D. J., and R. B. Smith, 2009: Orographic precipitation in the tropics: large-eddy simulations and theory. *J. Atmos. Sci.*, **66**, 2559-2578.

Kuo, Y.-H., and G. T.-J. Chen, 1990: The Taiwan area mesoscale experiment (TAMEX): an overview. *Bull. Amer. Meteor. Soc.*, **71**, 4, 488-503.

Muhlbauer, A. and U. Lohmann; 2008, Sensitivity studies of the role of aerosols in warm-phase orographic precipitation in different dynamical flow regimes, *J. Atmos. Sci.*, **65**, 2522-2542

Morrison, H., and W. W. Grabowski, 2007: Comparison of bulk and bin warm-rain microphysics models using a kinematic framework. *J. Atmos. Sci.*, **64**, 8, 2839-2861.

Nicholls, S., and M. A. Lemone, 1980: The fair weather boundary layer in GATE: The relationship of subcloud fluxes and structure to the distribution and enhancement of cumulus clouds. *J. Atmos. Sci*., **37**, 9, 2051-2067.

Paluch, I. R., and D. H. Lenschow, 1991: Stratiform cloud formation in the marine boundary layer. *J. Atmos. Sci.*, **48**, 19, 2141–2158.

Rauber, R. M., and Coauthors, 2007: Rain in (shallow) cumulus over the ocean: The RICO campaign. *Bull. Amer. Meteor. Soc*., **88**, 12, 1912-1928.

Reisner, J. M., and P. K. Smolarkiewicz, 1994: Thermally forced low Froude number past three-dimensional obstacles. *J. Atmos. Sci.,* **51,** 1, 117-133.

Robinson, F. J., S. C. Sherwood, D. Gerstle, C. Liu, and D. J. Kirshbaum, 2011: Exploring the land-ocean contrast in convective vigor using islands. *J. Atmos. Sci.*, **68**, 3, 602-618.

Roe, G. H., 2005: Orographic Precipitation. *Annu. Rev. Earth Planet. Sci.,* **33**, 645-671.

Rotunno, R., and R. A. Houze, 2007: Lessons on orographic precipitation from the Mesoscale Alpine Programme. *Quart. J. Roy. Meteor. Soc.,* **133**, 811-830.

Schär, C., and R. B. Smith, 1993: Shallow-water flow past isolated topography. Part I: Vorticity production and wake formation. *J. Atmos. Sci.,* **50**, 10, 1373-1400.

Siebesma, A. P., and Coauthors, 2003: A large eddy simulation intercomparison study of shallow cumulus convection. *J. Atmos. Sci.,* **60**, 10, 1201-1219.

Shinoda, T., and Coauthors, 2009: Structure of convective circulation in the atmospheric boundary layer over the Northwestern Pacific Ocean under a subtropical high. *J. Meteor. Soc. Japan*, **87**, 6, 979-996.

Smith, RB, 1979 The influence of mountains on the atmosphere. B. Saltzman, Ed., *Adv Geophys.*, **21,** 87-230.

Smith, RB. 1987. Aerial observations of the Yugoslavian Bora. *Journal of the Atmospheric Sciences* 44 (2): 269-297

Smith, R. B., A. C. Gleason, P. A. Gluhosky, and V. Grubisic, 1997: The wake of St. Vincent. *J. Atmos. Sci*., **54**, 5, 606-623.

Smith, R. B., 2006. Progress on the theory of orographic precipitation. Chapter 1 in *Special Paper 398: Tectonics, Climate, And Landscape Evolution*, edited by S. D. Willett, N. Hovius, M. Brandon, and D. Fisher, Geological Society of America, 1-16.
Chapter in a book?

Smith, R. B., P. Schafer, D. J. Kirshbaum, E. Regina, 2009a: Orographic precipitation in the tropics: experiments in Dominica. *J. Atmos. Sci*., **66**, 1698-1716.

Smith, R. B., P. Schafer, D. J. Kirshbaum, E. Regina, 2009b: Orographic enhancement of precipitation inside Hurricane Dean. *J. Hydrometeorol*., **10**, 820-831.

Sobel, A. H., C. D. Burleyson, and S. E. Yuter, 2011: Rain on small tropical islands. *J. Geophys. Res.*, **116**, D08102

Stoelinga, M. T., and Coauthors, 2003: Improvement of microphysical parameterization through observational verification experiment. *Bull. Amer. Meteor. Soc*., **84**, 12, 1807-1826.

Wang, L.-P., and W. W. Grabowski, 2009: The role of air turbulence in warm rain initiation. *Atmos. Sci. Lett.,* **10**, 1, 1-8.

Wang, Z, P. Wechsler, W Kuester, J. French, A.Rodi, B. Glover, M. Burkhart, D. Lukens, 2009, Wyoming Cloud Lidar: instrument description and applications, *Optics Express*, **17**, 13576-13587

Wratt, D. S., and Coauthors, 1996: The New Zealand Southern Alps experiment. *Bull. Amer. Meteor. Soc*., **77**, 4, 683-692.

Warner, J., 1968: A reduction in rainfall associated with smoke from sugar-cane fires - An inadvertent weather modification? *J. Appl. Meteor.*, **7**, 247- 251.

Wilson, J. W., R. E. Carbone, J. Tuttle, and T. D. Keenan, 2001: Tropical island convection in the absence of significant topography. Part II: Nowcasting storm evolution. *Mon. Wea. Rev.*, **129**, 1637–1655.

Woodcock, A. H., 1960: The origin of trade-wind orographic shower rains. *Tellus*, **12**, 3, 315-326.

Yang, Y., Y.-L. Chen, 2008: Effects of terrain heights and sizes on island-scale circulations and rainfall for the island of Hawaii during HaRP. *Mon. Wea. Rev.*, **136**, 120-146.

10. Figures Captions

1. Landsat-7 image of Dominica in February 2000 (Day of year=50). Airflow is from right to left. Cumulus rolls were amplified over the island.

2. Guadeloupe Radar (TFFR) derived map of annual rainfall for Dominica for 2007. (from Smith et al. 2009). Units are mm/day. Note the small upstream enhancement and dry rain shadow.

3. Dominica Terrain, deployed instruments and King Air flight tracks 1 through 6. The altitudes of each leg are given. Typical order of legs was 1L, 2L, 1H, 2H, 3, 4, 3, 4, 5, 6.

4. Temperature, precipitation and trade wind speed during DOMEX2011. Solid curves are from the FWL mountain weather station. The symbols are from upstream aircraft data. Dashed green line is the average precipitation rate over Dominica derived from the Guadeloupe radar. Note the period from April 14 to 20 with weak wind and precipitation and increased diurnal temperature range.

5. Role of ambient tradewind speed on a) convection intensity on Leg 3 (linear fit for U>5 only) , b) Aerosol number concentration on Leg 3, c) Cloud particle number concentration on leg 3, d) Upper wind divergence between Legs 3 and 4 at z=1700m

6. Upstream aircraft soundings for the low wind (RF07) and high wind (RF13) cases. a) cross-mountain wind speed, b) potential and equivalent potential temperature. Note the reverse shear and the conditional instability.

7. Photographs of Dominica convection taken from the King Air for a weak and strong wind case: a) RF07 , b) RF13

8. Precipitation over Dominica for the four-hour flight period from the Guadeloupe radar. a) low wind case (RF07), b) high wind case (RF13). Note change in color scale.

9. Horizontal winds at z=1700m a) low wind case (RF07), b) high wind case (RF13). With low ambient winds, winds diverge from convective detrainment while with high ambient winds wind appear to converge flow from lee-side plunging.

10. Reflectivity from the 95 GHz Wyoming Cloud radar on upwind Leg 3. a) low wind case (RF07), b) high wind case (RF13). The high wind case has much stronger reflectivity but some beam attenuation too.
11. Reflectivity from the 95GHz Wyoming Cloud Radar on downwind Leg 4. a) low wind case (RF07), b) high wind case (RF13). The high wind case shows spillover and “book-end” convection.

12. The probability density for mean droplet size for the low wind (RF07) and high wind (RF13) cases. The breadth of each peak is mostly due to entrainment. The shift arises from island source aerosols on the low wind day.

13. CO_2 and aerosol for the racetrack leg sequence 3,4,3,4 at z=1700m, outside of cloud. a) low wind case (RF07), b) high wind case (RF13). Leg numbers indicate the middle of each leg when the aircraft is over the island. Island terrain is shown at the bottom. On the low wind day, the convection seems to be detraining aerosol enriched and CO_2 depleted air.

14. Scatter diagram for temperature and specific humidity along Leg 1L at z=300m for RF07. The reference line represents constant virtual temperature and therefore constant buoyancy. The cooler wetter parcels in the lower right of the cluster may be the seeds of the island convection. The steep line with slope L/Cp indicates how the points would scatter if the cause of the variation was evaporating rainfall.

15. Schematic of the two types of convection found over Dominica. a) diurnal thermal convection found with weak trade winds; b) mechanically driven convection found with strong trade winds. Heavy up-arrows are the strongest updrafts. The heavy down arrow and curved dotted streamline show the plunging flow over the lee slopes. Thin arrows show the origin of buoyancy. Filled dots are aircraft legs into the page. Symbols S, T and W describe measured properties of the flow: S= humid seeds for convection; T=island derived tracer; W=wake. Inverted Vs indicate clear air turbulence.

Table 1: Typical flow parameters and characteristics for low and high wind cases.

Properties	**Data/Legs**	**Low Wind Class**	**High Wind Class**
Research Flights		7,8	12,13,16,17
Wind speed	1L, Station*	$2\ to\ 4\ m\ s^{-1}$	$9\ to\ 12\ m\ s^{-1}$
Wind direction	1L	easterly	easterly
Critical level (U=0)	Sounding	$\sim 1500m$	$\sim 3200m$
Shear (dU/dz)	Sounding	$\sim 0.003 s^{-1}$	$\sim 0.003 s^{-1}$
Dry stability ($d\theta/dz$)	Sounding	$\sim +5K\ km^{-1}$	$\sim +5K\ km^{-1}$
Moist stability ($d\theta_E/dz$)	Sounding	$\sim -6K\ km^{-1}$	$\sim -5K\ km^{-1}$
Non-dimensional Mountain height ($\hat{h}$)	$\hat{h} = hN/U$	3	0.9
Max precipitation	radar	1mm	15mm
Lofted island tracers	Legs 3 and 4	yes	no
Plunging flow	Camera and Leg 4	no	yes
Wake	Leg 5	no	yes
Diurnal T range	Station*	8°C	3°C
Cloud fraction %	Leg 3	8 to 13	**16 to 22**
"	Leg 4	**20 to 32**	1 to 5
STD(w') ($m\ s^{-1}$)	Leg 3	.7 to .8	.6 to 1.1
"	Leg 4	1.1 to 1.3	.8 to 1.4
Skewness of w'	Leg 3	-0.1 to 0.3	**1.5 to 2.5**
"	Leg 4	**1.0 to 1.5**	0.0 to 0.4
Latent Heat Flux ($W\ m^{-2}$)	Leg 3	60 to 310	**180 to 800**
"	Leg 4	**800 to 1400**	-20 to 400
Cloud number concentration (cm^{-3})	Leg 3	**110 to 130**	50 to 70
"	Leg 4	**190 to 270**	30 to 80
Mean cloud particle diameter (μm)	Leg 3	13 to 15	**19 to 21**
"	Leg 4	12 to 13	**19 to 21**

(*Station=mountain weather station)

Rendered Figure
Click here to download Rendered Figure: FigureFile.docx

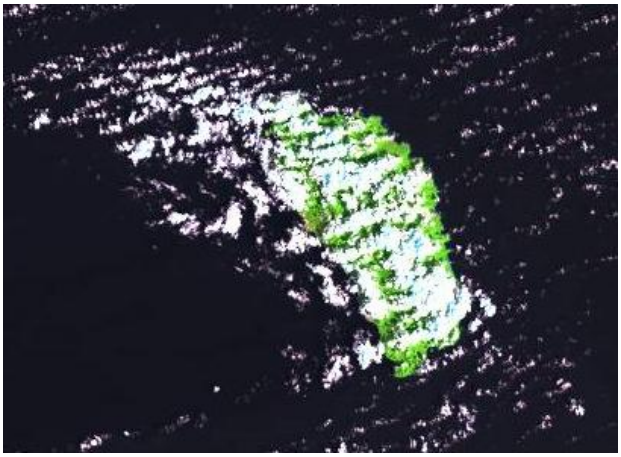

Fig 1: Landsat-7 image of Dominica in February 2000 (Day of year=50). Airflow is from right to left. Cumulus rolls were amplified over the island.

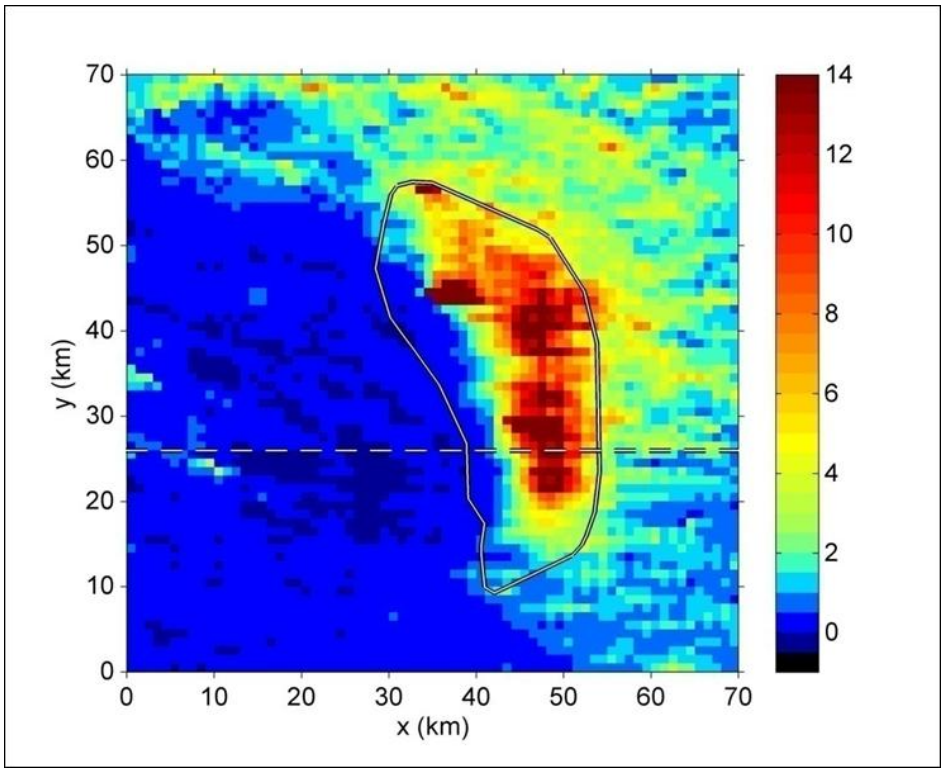

Figure 2: Guadeloupe Radar (TFFR) derived map of annual rainfall for Dominica for 2007. (from Smith et al. 2009). Units are mm/day. Note the small upstream enhancement and dry rain shadow.

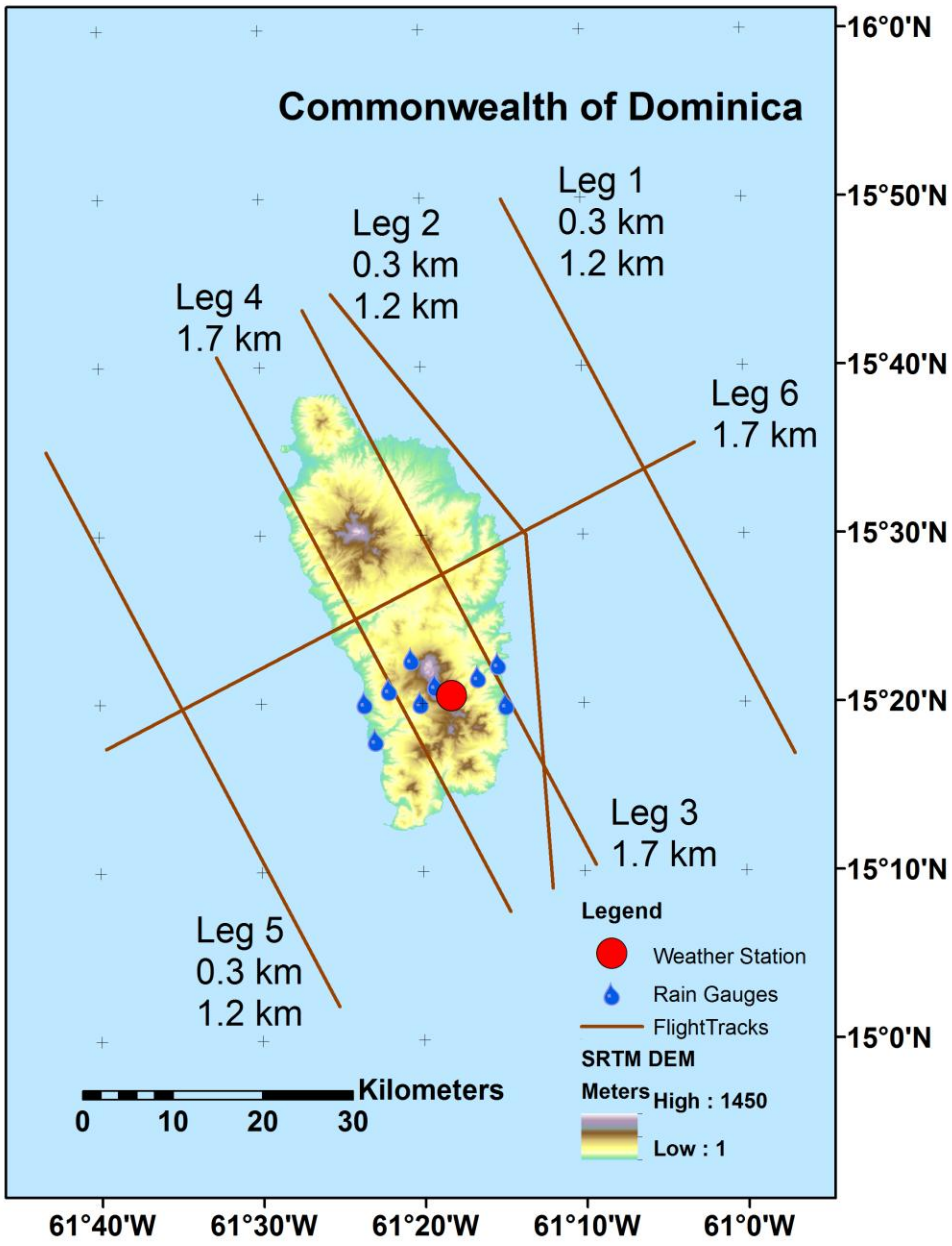

Figure 3: Dominica Terrain, deployed instruments and King Air flight tracks 1 through 6. The altitudes of each leg are given. Typical order of legs was 1L, 2L, 1H, 2H, 3, 4, 3, 4, 5, 6.

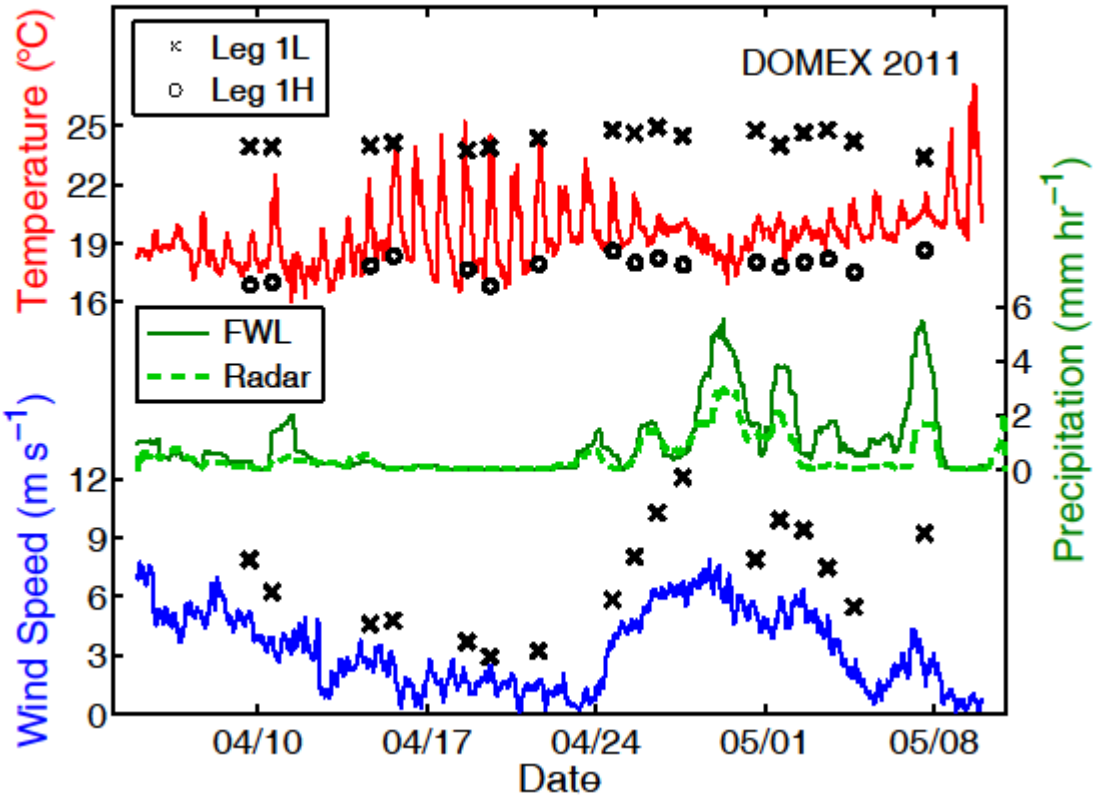

Figure 4: Temperature, precipitation and trade wind speed during DOMEX2011. Solid curves are from the FWL mountain weather station. The symbols are from upstream aircraft data. Dashed green line is the average precipitation rate over Dominica derived from the Guadeloupe radar. Note the period from April 14 to 20 with weak wind and precipitation and increased diurnal temperature range.

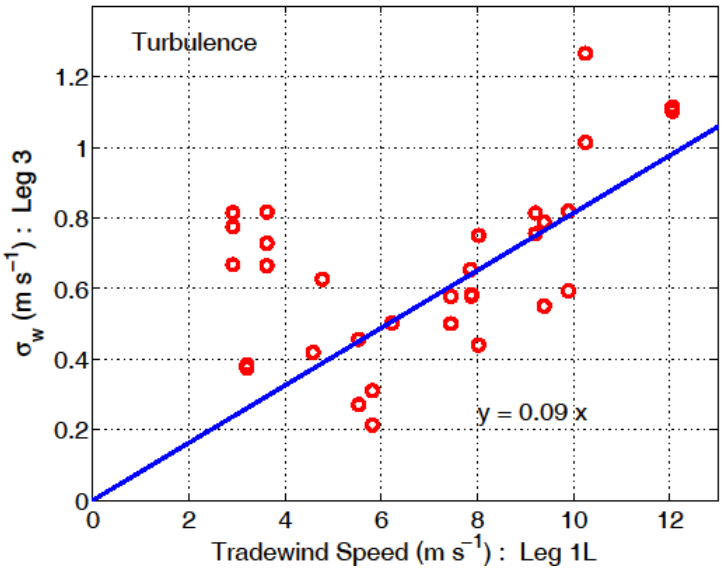
Turbulence
y = 0.09 x
σw (m s−1) : Leg 3
Tradewind Speed (m s−1) : Leg 1L
0
0.2
0.4
0.6
0.8
1
1.2
0
2
4
6
8
10
12

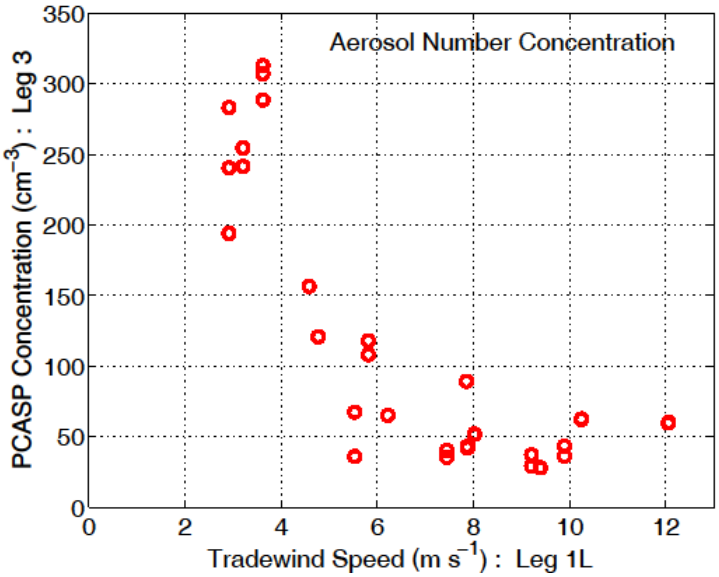
Aerosol Number Concentration
PCASP Concentration (cm−3) : Leg 3
Tradewind Speed (m s−1) : Leg 1L
0
50
100
150
200
250
300
350
0
2
4
6
8
10
12

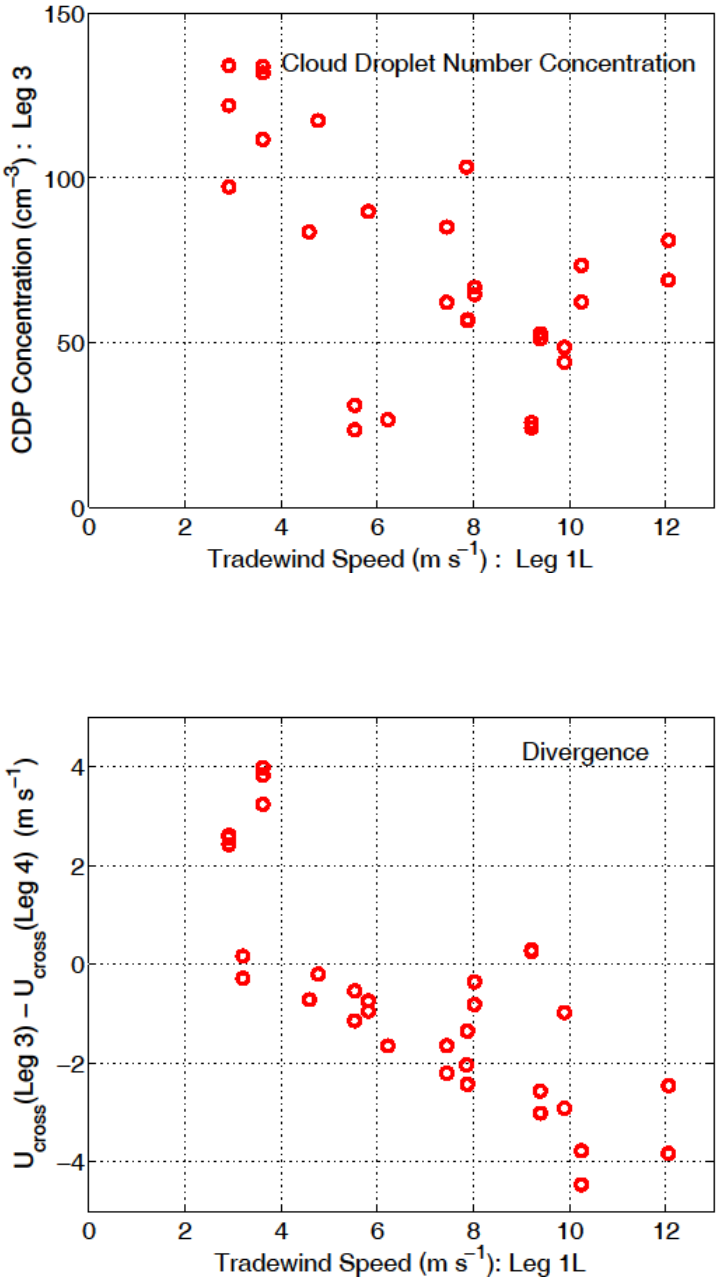

Figure 5: Role of ambient tradewind speed on a) convection intensity on Leg 3 (fit for U>5 only) , b) Aerosol number concentration on Leg 3, c) Cloud particle number concentration on leg 3, d) Upper wind divergence between Legs 3 and 4 at z=1700m

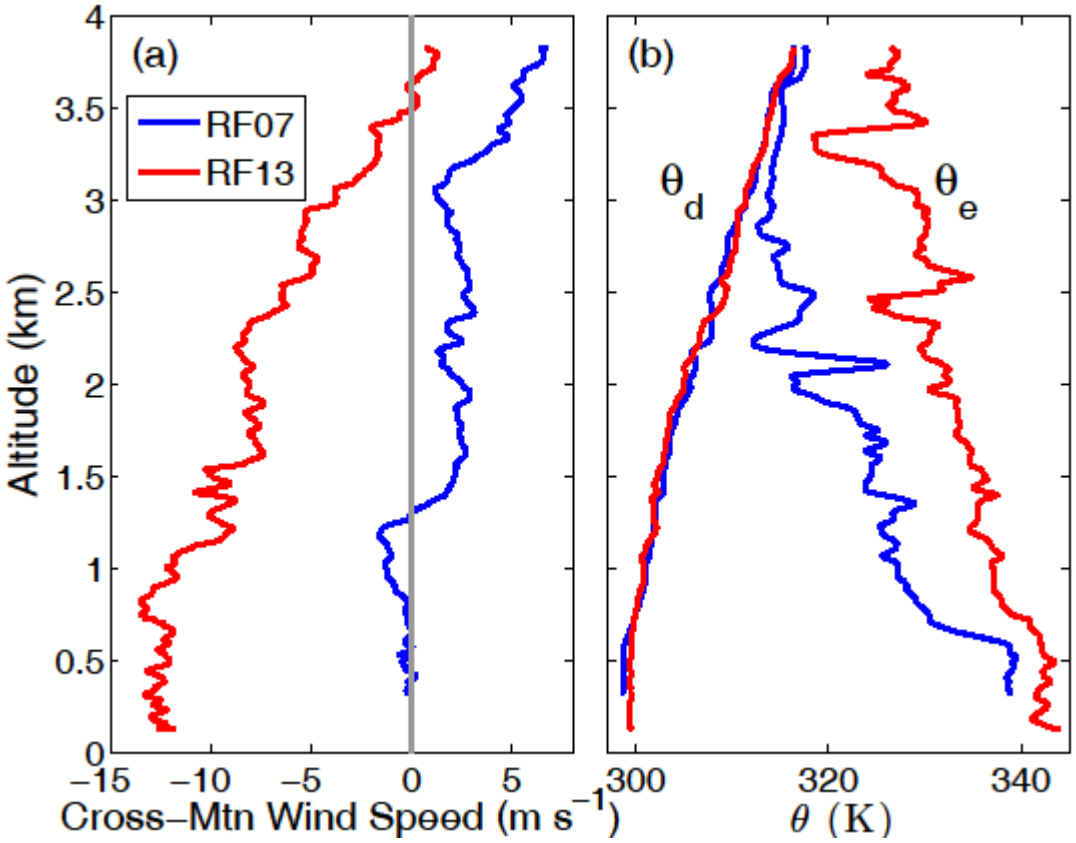

Figure 6: Upstream aircraft soundings for the low wind (RF07) and high wind (RF13) cases. a) cross-mountain wind speed, b) the dry potential temperature and the equivalent potential temperature. Note the reverse shear and the conditional instability.

Figure 7: Photographs of Dominica convection taken from the King Air for a weak and strong wind case: a) RF07 , b) RF13. The view is to the west.

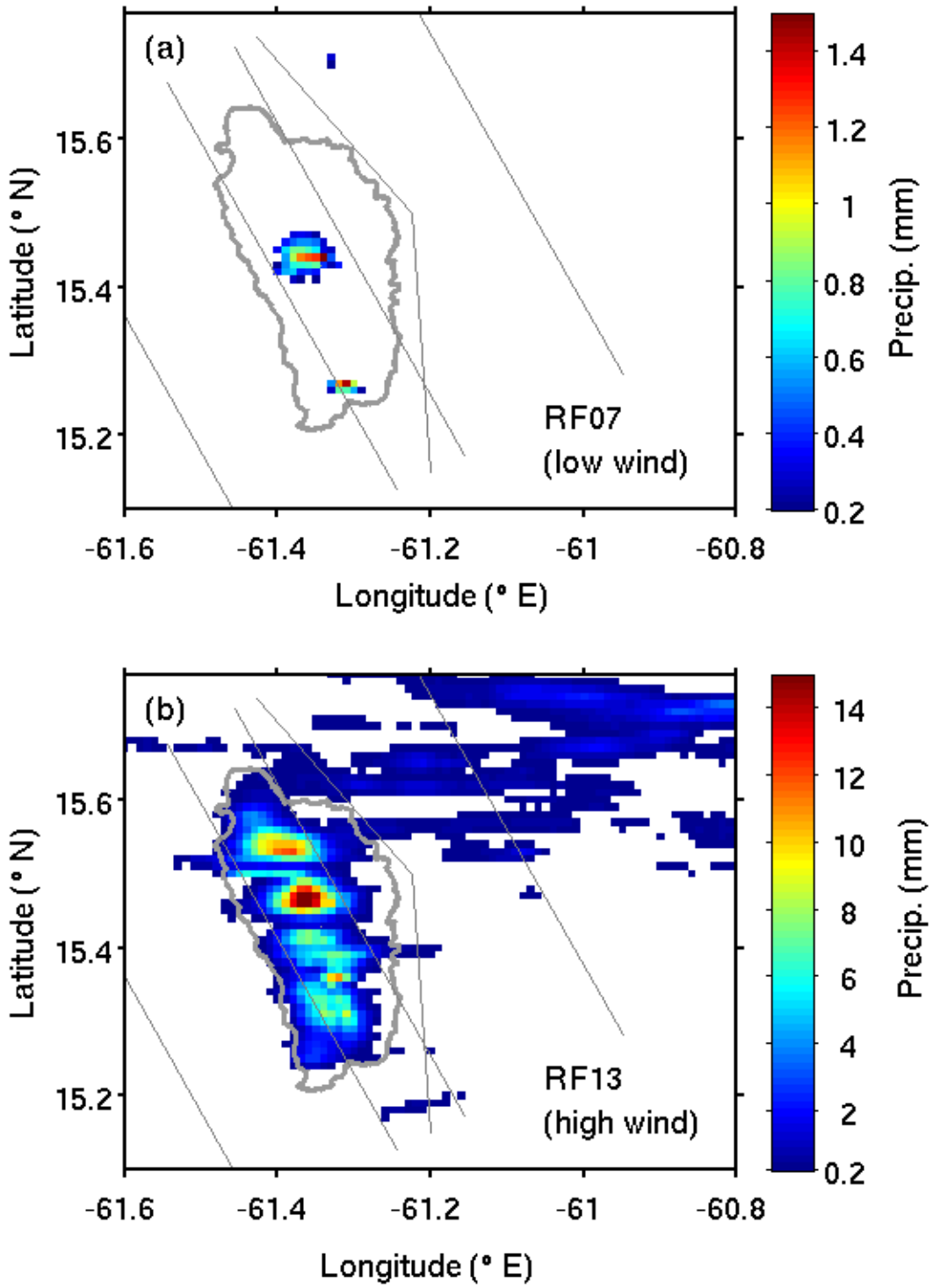

Figure 8: Precipitation over Dominica for the four-hour flight period from the Guadeloupe radar. a) low wind case (RF07), b) high wind case (RF13). Note change in color scale.

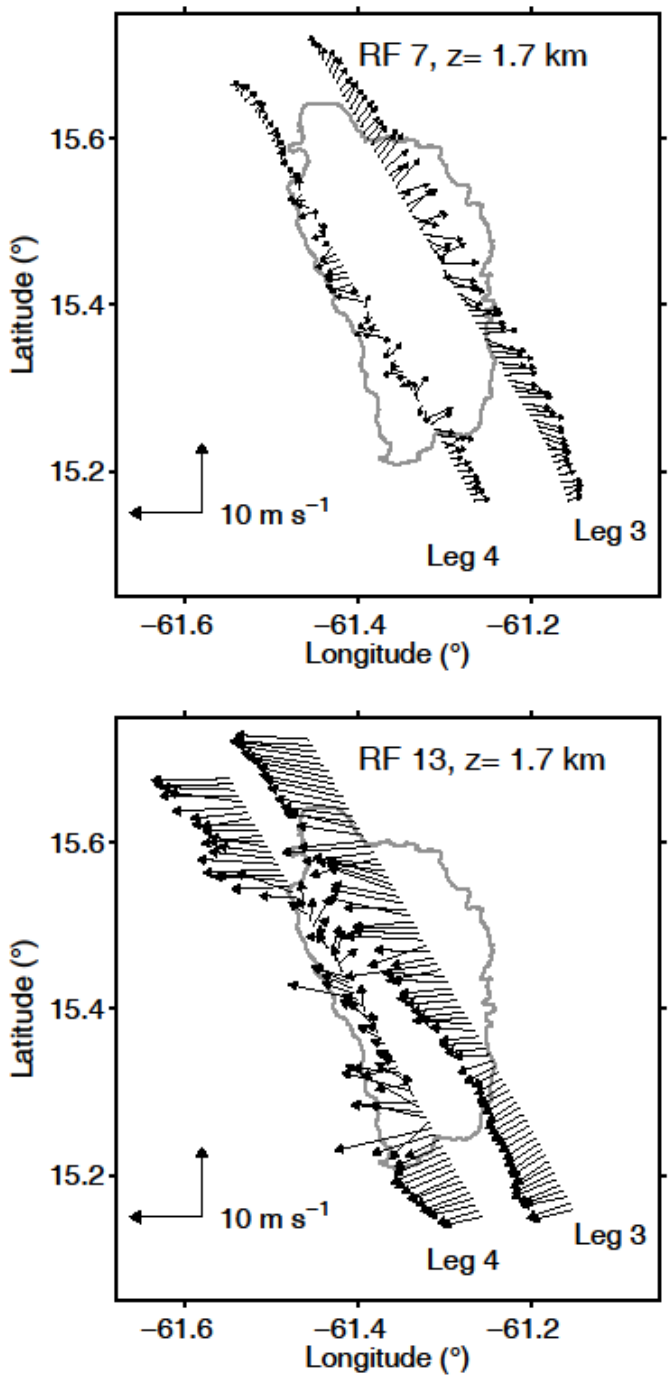

Figure 9: Horizontal winds at z=1700m a) low wind case (RF07), b) high wind case (RF13). With low ambient winds, winds diverge from convective detrainment while with high ambient winds wind appear to converge flow from lee-side plunging.

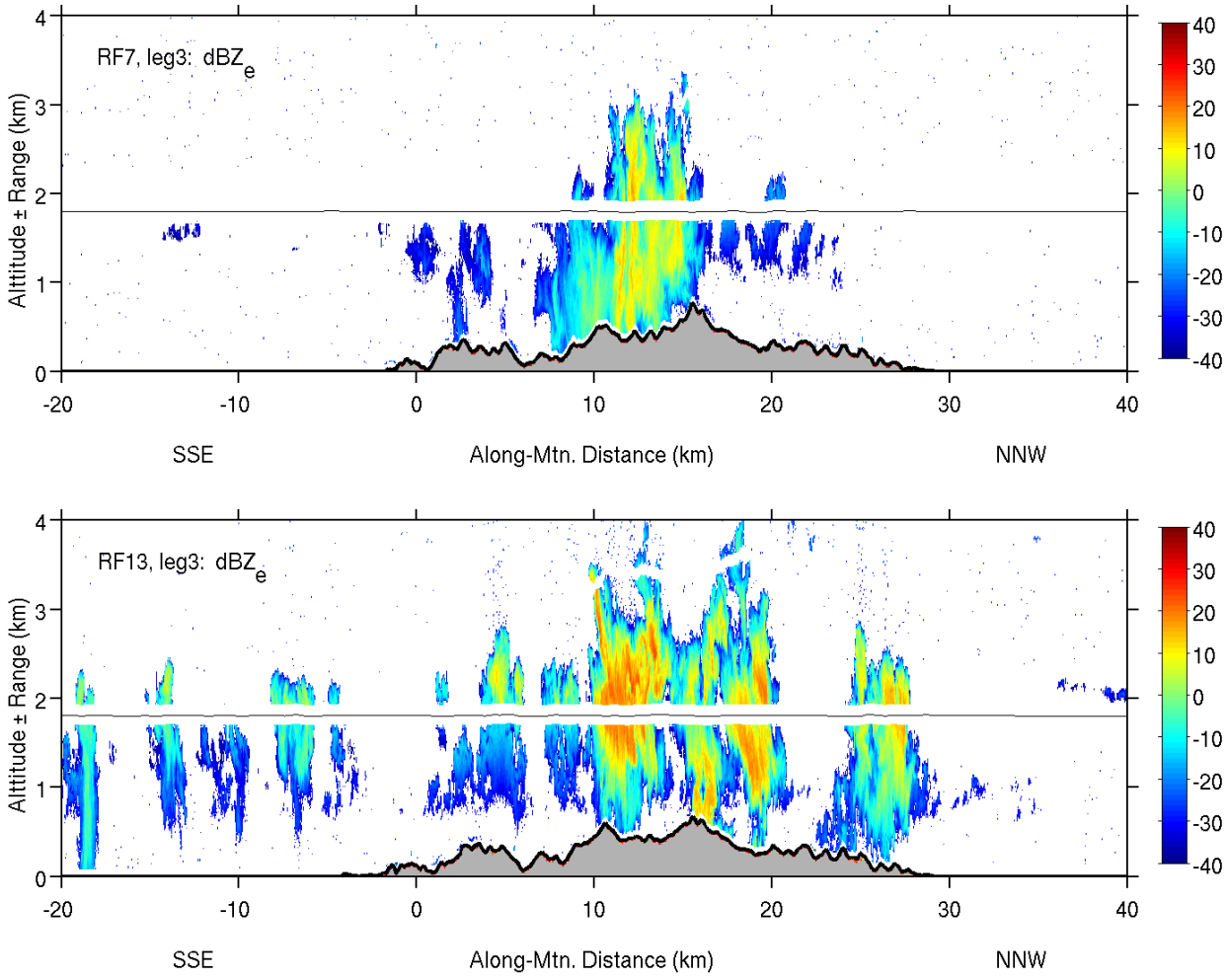

Figure 10: Reflectivity from the 95 GHz Wyoming Cloud radar on upwind Leg 3. a) low wind case (RF07), b) high wind case (RF13). The high wind case has much stronger reflectivity but some beam attenuation too.

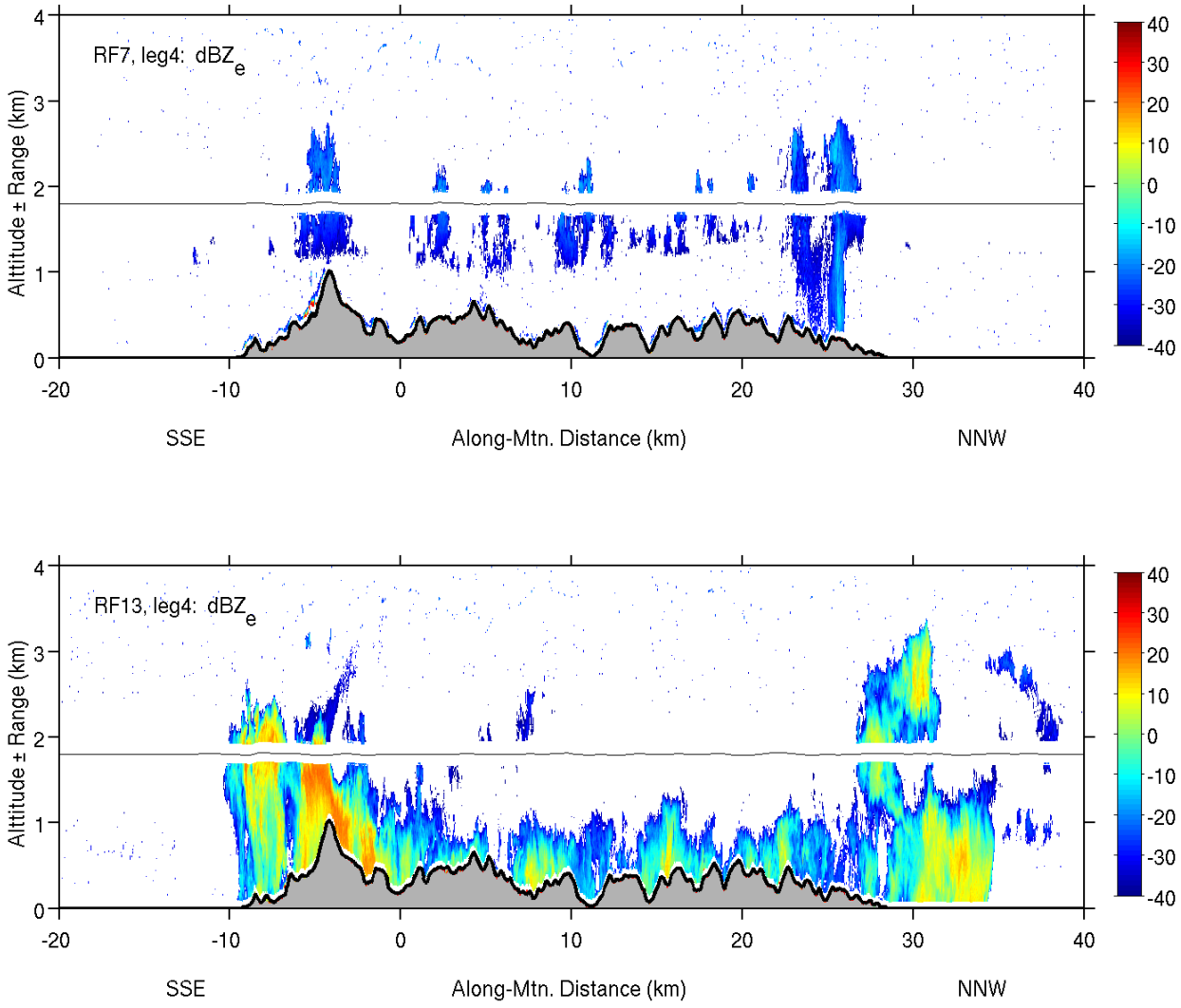

Figure 11: Reflectivity from the 95GHz Wyoming Cloud Radar on downwind Leg 4. a) low wind case (RF07), b) high wind case (RF13). The high wind case shows spillover and "book-end" convection.

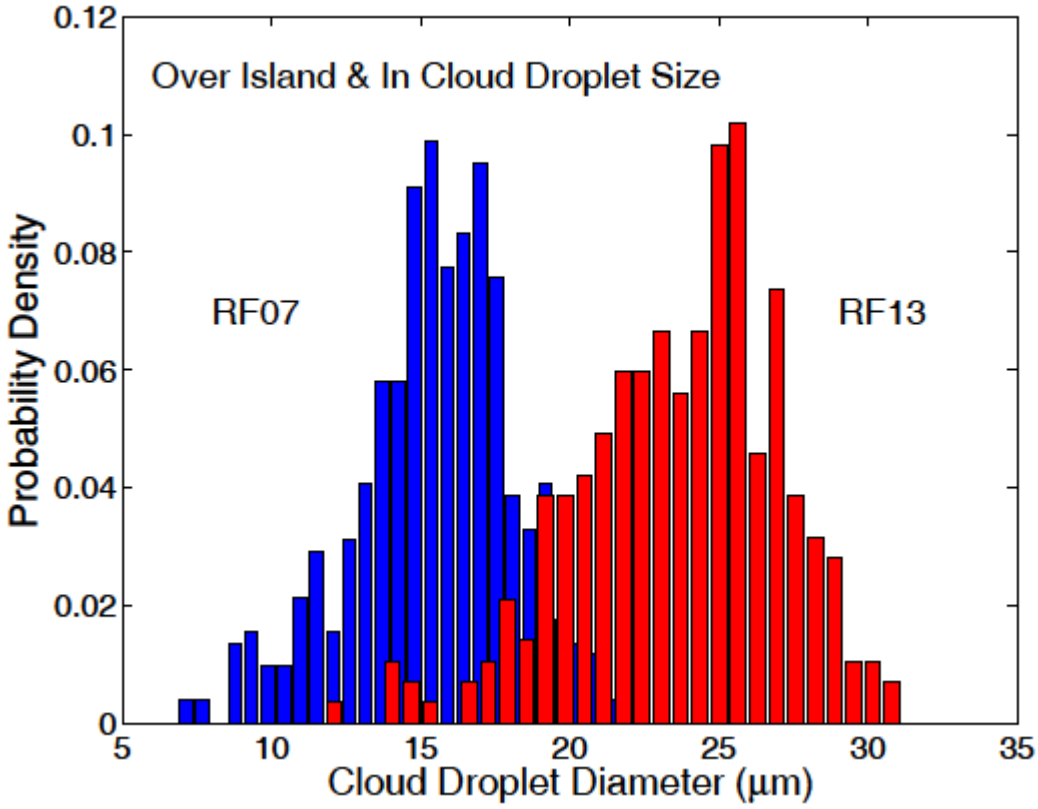

Figure 12: The probability density for mean droplet size for the low wind (RF07) and high wind (RF13) cases. The breadth of each peak is mostly due to entrainment. The shift arises from island source aerosols on the low wind day.

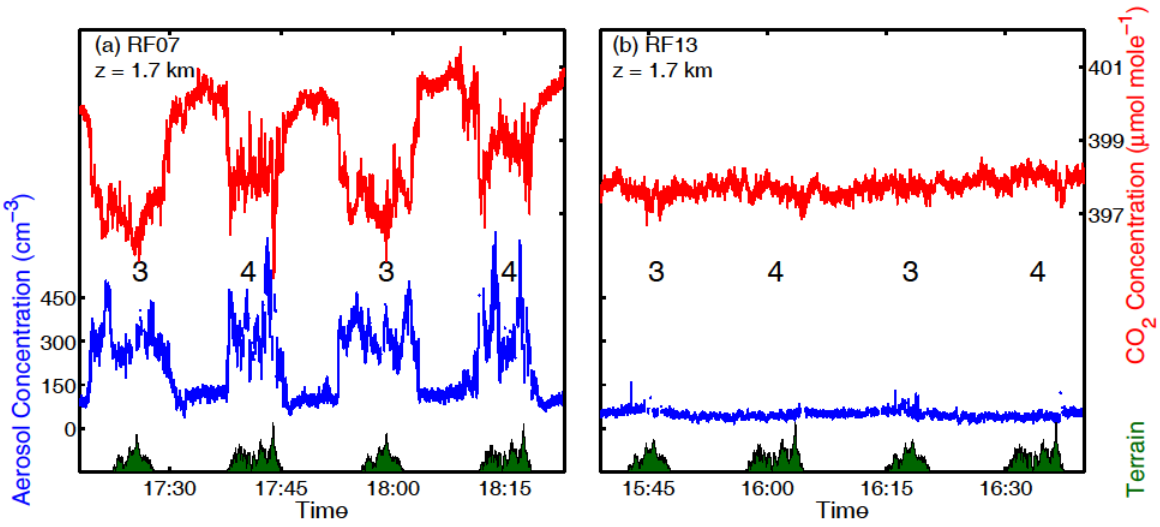

Figure 13: CO_2 and aerosol for the racetrack leg sequence 3,4,3,4 at z=1700m, outside of cloud. a) low wind case (RF07), b) high wind case (RF13). Leg numbers indicate the middle of each leg when the aircraft is over the island. Island terrain is shown at the bottom. On the low wind day, the convection seems to be detraining aerosol enriched and CO_2 depleted air.

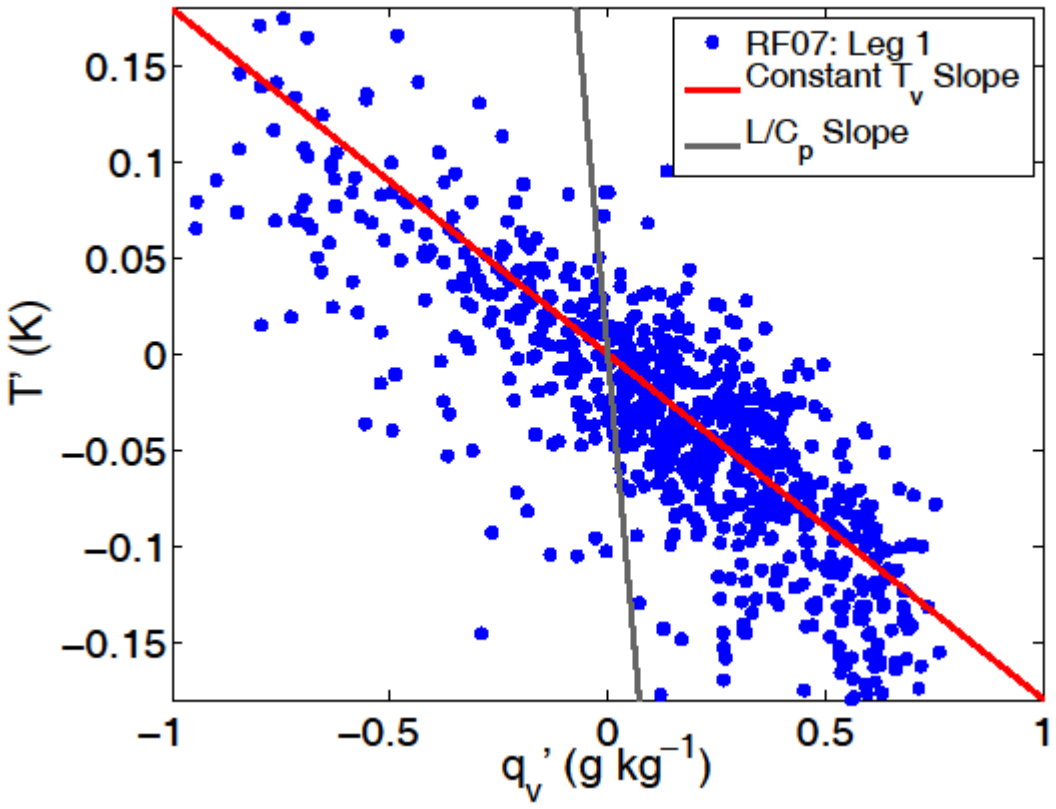

Figure 14: Scatter diagram for temperature and specific humidity upwind of Dominica along Leg 1L at z=300m for a low wind day (RF07). The red reference line represents constant virtual temperature and therefore constant buoyancy. The cooler wetter parcels in the lower right of the cluster may be the seeds of the island convection. The steep line with slope L/Cp indicates how the points would scatter if the cause of the variation was evaporating rainfall.

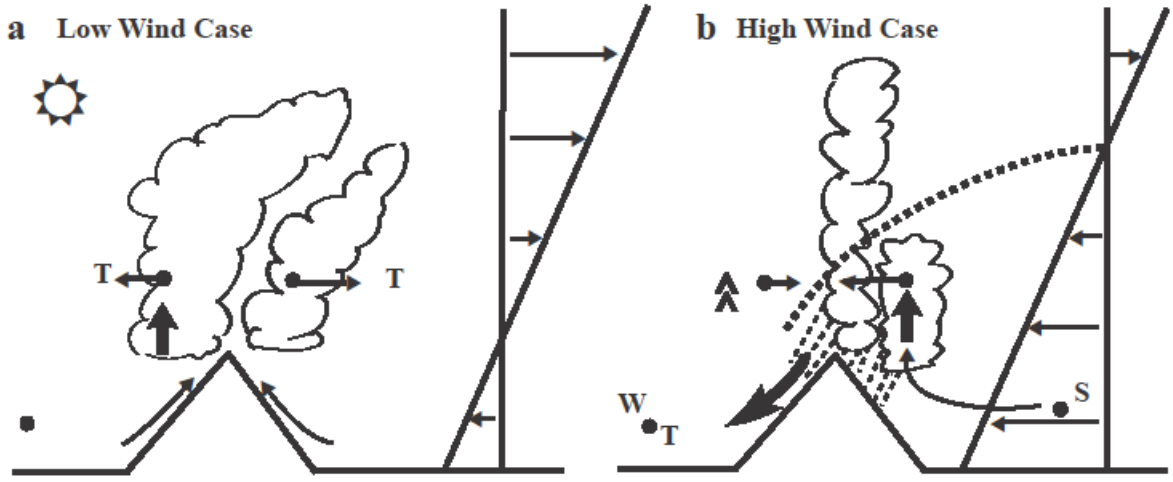

Figure 15: Schematic of the two types of convection found over Dominica. a) diurnal thermal convection found with weak trade winds; b) mechanically driven convection found with strong trade winds. Heavy up-arrows are the strongest updrafts. The heavy down arrow and curved dotted streamline show the plunging flow over the lee slopes. Thin arrows show the origin of buoyancy. Filled dots are aircraft legs into the page. Symbols S, T and W describe measured properties of the flow: S= humid seeds for convection; T=island derived tracer; W=wake. Inverted Vs indicate clear air turbulence.